SAND2020-3824C

Cathodic Reduction Kinetics on Stainless Steel Surfaces in Marine Environments

Jacob Carpenter
Materials Reliability, Sandia National Laboratories, Albuquerque, New Mexico 87123, USA

Objectives

- Predict cathode kinetics in marine atmospheric system over long time scales to be used for life-time predictions
- Provide kinetic inputs for the Chen-Kelly model for maximum pit sizes
- Determine the cathode kinetics of SS304L using rotating disk electrode polarizations, cyclic voltammetry and surface state characterization methods.

Why Study High pH Atmospheric Corrosion Systems?

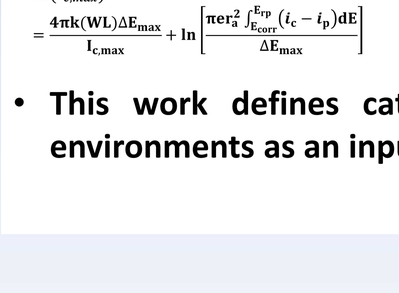

Figure 1: Dry casks used for permanent storage of spent nuclear fuel

- High chloride brine possible on metal surfaces.
- Long time cathode kinetics:
  - (HER) $(2H_2O + 4e^- \rightarrow 2OH^- + H_2)$
  - (ORR) $(O_2 + 2H_2O + 4e^- \rightarrow 4OH^-)$
- The reaction energies, potentials and ultimate reaction rates will all change with pH.

Figure 2: The locations of spent fuel storage sights

pH Evolution in a Droplet Environment

- Droplet displays higher pH on the edges than in center which can be characteristic of anode-cathode development

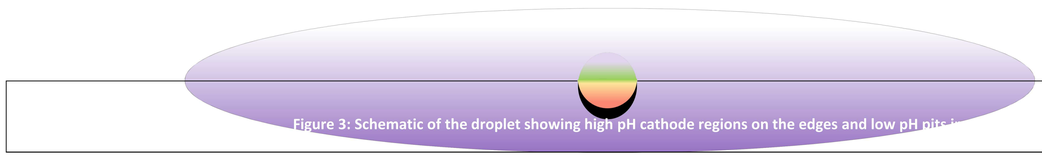

Figure 3: Schematic of the droplet showing high pH cathode regions on the edges and low pH pits in

Figure 4 (right): 86% RH Seawater droplet on a SS304L coupon was kept at humidity for 24 hours. Universal indicator was added at the end.

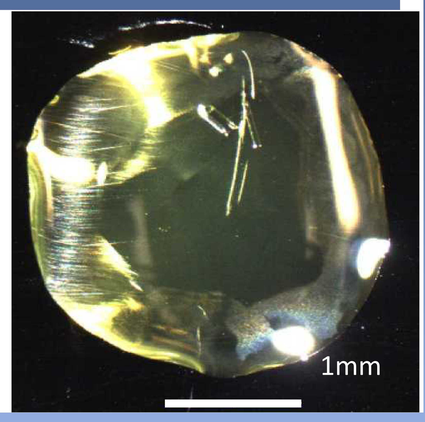

Solution Effects on Cathode Kinetics

- The reaction energies and Nernst potentials of the system will change according to the amount of NaOH in the system
- The pH of the solution can affect the electron transfer number (n)

- A change in the kinetics can lead to a change in the available cathode current

$$\ln\left(\frac{i}{i_0}\right) \sim \frac{\alpha n F}{RT}(E - E_N)$$

Figure 5: Polarization curves on 304L steel in various solutions of sodium hydroxide. Up to pH 15.11

- The pH 15.1 curve does not fit the trend

Result: at high $pH, n \downarrow, \therefore\ i_{cath} \downarrow$

Rotation Speed Effects on Cathode Kinetics

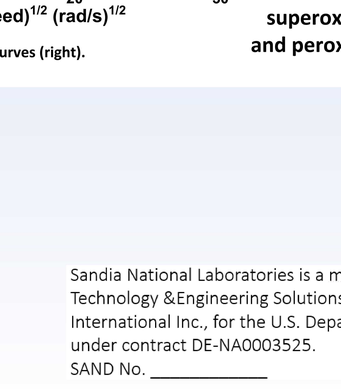

Figure 7: A schematic of a rotating disk electrode
ω – Rotation speed
δ – Mass transfer layer thickness
J_{O_2} - Oxygen species flux ($\propto i_{lim}$)

- Brine thickness has an important effect on the cathode kinetics.
- $WL \sim \delta = f(\omega)$

$$\delta = 1.61\, D^{\frac{1}{3}} \nu^{\frac{1}{6}} \omega^{-\frac{1}{2}}$$

$$i_{lim} = \frac{nFC_{O_2}D_{O_2}}{\delta}$$

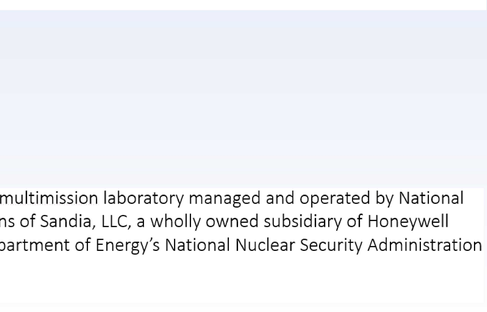

Figure 8: A family of polarization curves showing the effect of the changing mass transfer layer thickness.

Result: $\omega \uparrow, \delta \downarrow$, so $i_{lim} \uparrow$
Just like other seawater systems

Chen-Kelly Maximum Pit Size Model Background

Figure 2: schematic diagrams of the maximum pit model with Cathode and anode kinetics

k – brine conductivity
WL – Brine thickness

$$ln(I_{c,max}) = \frac{4\pi k(WL)\Delta E_{max}}{I_{c,max}} + \ln\left[\frac{\pi e r_a^2 \int_{E_{corr}}^{E_{rp}} (i_c - i_p)dE}{\Delta E_{max}}\right]$$

- Conservation of Charge
  - anodic demand relies on cathodic supply

- **This work defines cathode kinetics in high pH environments as an input for the Chen-Kelly Model**

Using Levich behavior to Determine Reaction Mechanisms

Figure 10: Graphs showing typical seawater Levich curves (left) compared to high pH Levich curves (right).

- The curves remain linear indicating maintenance of mass transfer control.
- Using the Levich slopes and known fluid properties, we can learn about the reaction mechanism

$$n = \frac{d(i_{lim})/d(\omega^{0.5})}{0.62\, nFC_{O_2}D_{O_2}^{\frac{2}{3}}\nu^{-\frac{1}{6}}}$$

Result:
For pH between 13.7 - 14.73
$$n = 1.46 \pm 0.14\ (95\%)$$

Because n is between 1 and 2, the mechanism of oxygen reduction likely is a mixture of the superoxide pathway (a) and peroxide pathway(b)

(a)
$$O_2 + e^- = O_2^-$$
$$O_2^- + 2H^+ + e^- = H_2O_2$$
(b)
$$O_2 + 2H^+ + 2e^- = H_2O_2$$
(both)
$$H_2O_2 + 2H^+ + 2e^- = 2H_2O$$

Sandia National Laboratories is a multimission laboratory managed and operated by National Technology &Engineering Solutions of Sandia, LLC, a wholly owned subsidiary of Honeywell International Inc., for the U.S. Department of Energy's National Nuclear Security Administration under contract DE-NA0003525.
SAND No. _____

Determining the Cathode Reaction at Ultra-high pH

Change in Reaction Mechanism

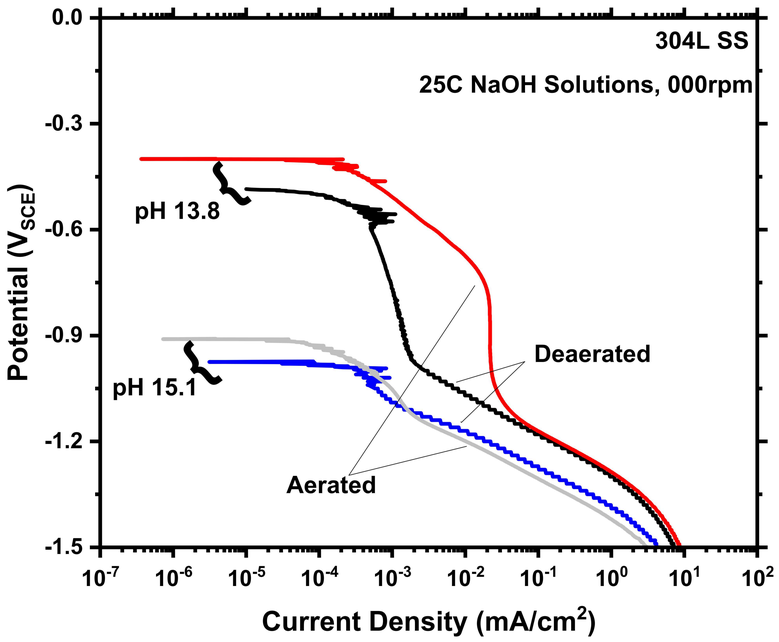

Figure 11: A polarization curve showing the effect of oxygen on a polarization curve. Solution was deaerated for four hours using lab-supplied nitrogen before the experiment.

- The presence or absence of oxygen does not change the kinetics in high pH systems. Oxygen is NOT the primary reactant in ultra-high pH systems.
- The dominant reaction at potentials far from the open circuit potential has not changed; It is still dominated by Water reduction (hydrogen evolution).

Result: ORR is not the dominant Cathode Reaction at ultra-high pH

Mechanism and Pourbaix Analysis

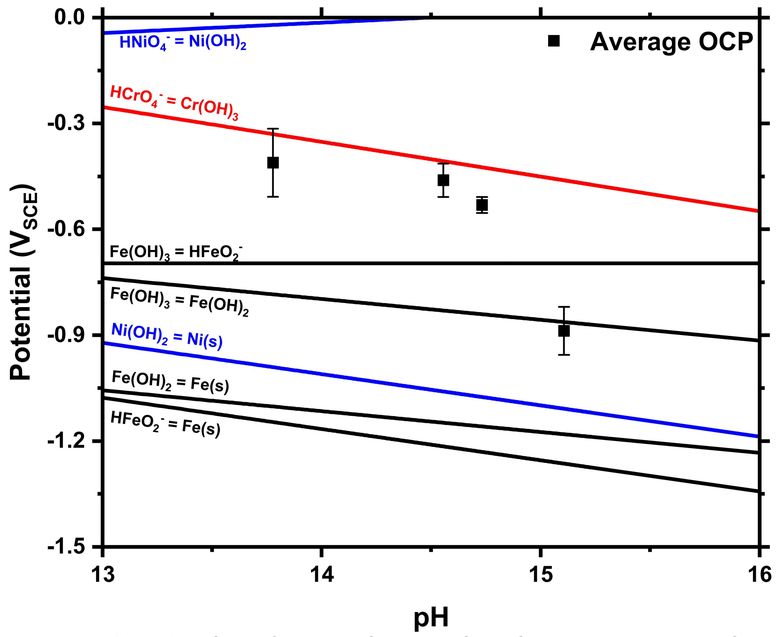

Figure 12: A Pourbaix diagram showing the relevant reactions in the system and The steady state potential of the system. All dominant ions are assumed to have a concentration of 1 µM

- The only major change in the state of the 304L SS is the change of the iron(III) passive film; Fe(OH)3 (OR FeO(OH)) is no longer solely dominant.
- Because the open circuit potential is so close to the potential for the passive film transition, the true surface state likely contains a mixture of Iron(III) and iron (II) passive films.
- The current at low overpotential likely comes from the dissolution of the Iron(III) by the following reactions:

$$FeO(OH)(s) + e^- = HFeO_2^-(aq) \quad (3)$$

$$FeO(OH)(s) + e^- = Fe(OH)_2(s) \quad (4)$$

Confirming the Cathode Reaction at high pH

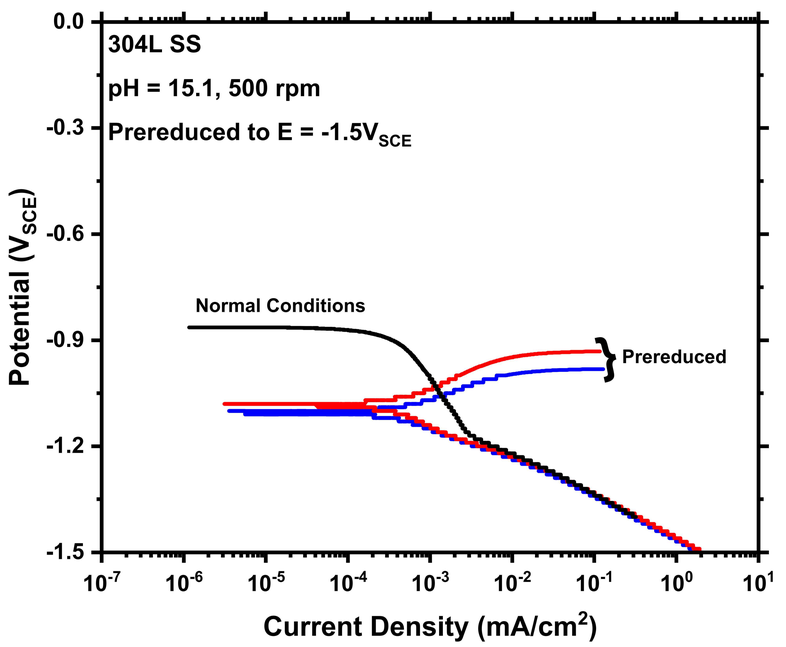

Figure 13: Polarization curves at ultra-high pH. Some curves were reduced beforehand at roughly -1.5V_{SCE}

- **By pre-reducing the surface, we remove the iron (III) passive film.**
- **The presence of the passive film greatly affects the current because the Iron (III) film is the source of the cathode current.**

Result: The Iron (III) passive film is very likely the source of the cathode current

Conclusions

Cathode Reaction Dominance Summary

	Close to OCP	Far From OCP
Low pH	Oxygen Reduction	Water Reduction
High pH	Fe(III) Conversion	Water Reduction

- In very high pH cathodes, the Iron (III) passive film breaks down into a less stable iron film ($Fe(OH)_2$) and iron (II) ions ($HFeO_2^-$)
- The kinetics of ORR slow down as pH increases from typical seawater.
- The electron transfer number for ORR on 304L stainless steel is constant at roughly 1.48 between pH 13.8 and 14.7

Implications

At high pH, less cathodic current may be available due to reduced kinetics in ORR and mixed reaction schemes, which could lead to smaller pit sizes

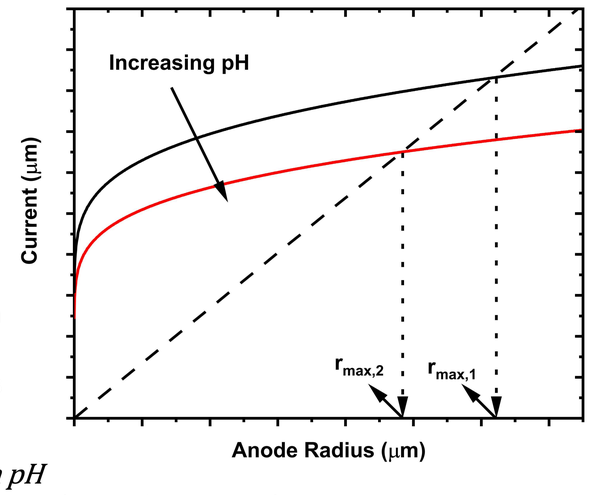

At high pH

$$n \downarrow, \therefore I_c \downarrow, implies\ r_{max} \downarrow$$

Future Work

Seawater Cathode Chemistry

Maximum Pit sizes

Affect of pH on Stress Corrosion Cracking and failure mechanisms

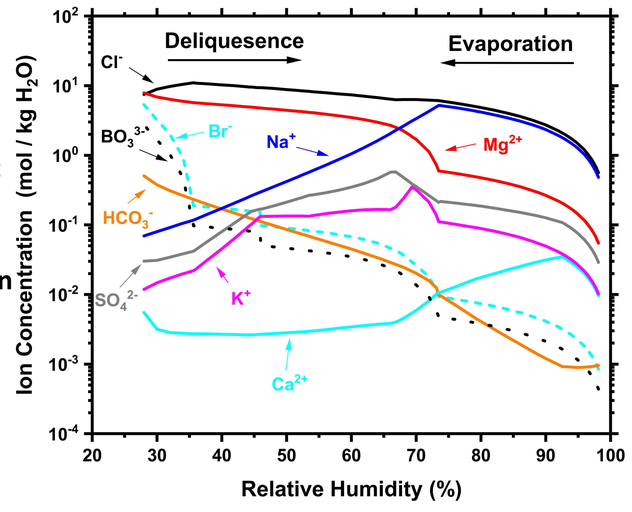

Acknowledgments

- I would like to thank Rebecca Schaller, Ryan Katona, and Eric Schindelholz for their guidance.
- Thank you to Timothy (TJ) Montoya and Jason (Jay) Taylor for his help with the experimental work
- Andrew Knight and Charles Bryan are also highly appreciated for their continued collaboration with our lab

References

1. Jin, W., Du, H., Zheng, S., Xu, H. & Zhang, Y. Comparison of the oxygen reduction reaction between NaOH and KOH solutions on a Pt electrode: The electrolyte-dependent effect. J. Phys. Chem. B 114, 6542–6548 (2010).
2. Zhang, P., Jin, H., Wang, T. & Wang, M. Insight into the effect of lithium-dendrite suppression by lithium bis(fluorosulfony)imide/1,2-dimethoxyethane electrolytes. Electrochim. Acta 277, 116–126 (2018).
3. Babić, R. & Metikoš-Huković, M. Oxygen reduction on stainless steel. J. Appl. Electrochem. 23, 352–357 (1993).
4. Chen, Z. Y. & Kelly, R. G. Computational modeling of bounding conditions for Pit size on stainless steel in atmospheric environments. J. Electrochem. Soc. 157, (2010).
5. Gojković, S. L. J., Zečević, S. K., Obradović, M. D. & Dražić, D. M. Oxygen reduction on a duplex stainless steel. Corros. Sci. 40, 849–860 (1998).
6. Striebel, K. A., McLarnon, F. R. & Cairns, E. J. Oxygen Reduction on Pt in Aqueous K2CO3 and KOH. J. Electrochem. Soc. 137, 3351–3359 (1990).
7. Weiss, R. F. Weiss et al 1970-The solubility of nitrogen, oxygen and argon in water and seawater.pdf. 17, (1970).
8. Zhang, H. L. & Han, S. J. Viscosity and density of water+sodium chloride+potassium chloride solutions at 298.15 K. J. Chem. Eng. Data 41, 516–520 (1996).
9. Geniès, L., Faure, R. & Durand, R. Electrochemical reduction of oxygen on platinum nanoparticles in alkaline media. Electrochim. Acta 44, 1317–1327 (1998).
10. Vázquez, G., Alvarez, E., Varela, R., Cancela, A. & Navaza, J. M. Density and viscosity of aqueous solutions of sodium dithionite, sodium hydroxide, sodium dithionite + sucrose, and sodium dithionite + sodium hydroxide + sucrose from 25 °C to 40°C. J. Chem. Eng. Data 41, 244–248 (1996).
11. Åkerlöf, G. & Kegeles, G. The Density of Aqueous Solutions of Sodium Hydroxide. J. Am. Chem. Soc. 61, 1027–1032 (1939).
12. Bourne, J. R., Dell'Ava, P., Dossenbach, O. & Post, T. Densities, Viscosities, and Diffusivities in Aqueous Sodium Hydroxide—Potassium Ferri and Ferrocyanide Solutions. J. Chem. Eng. Data 30, 160–163 (1985).
13. Tromans, D. Concentration , Temperature and Pressure Effects. Met. Mater. 279–296 (1998).
14. Tromans, D. Oxygen in Water : a Thermodynamic Analysis. Hydrometallurgy 48, 327–342 (1998).
15. Carpenter, J., Katona, R. & Schindelholz, E. Cathodic Reduction Kinetics on Stainless Steel Surfaces in Corrosive Low Humidity Environments. 877, 2018 (2019).
16. Chatenet, M., Molina-Concha, M. B., El-Kissi, N., Parrour, G. & Diard, J. P. Direct rotating ring-disk measurement of the sodium borohydride diffusion coefficient in sodium hydroxide solutions. Electrochim. Acta 54, 4426–4435 (2009).
17. Alexander, C. L. et al. Oxygen Reduction on Stainless Steel in Concentrated Chloride Media. J. Electrochem. Soc. 165, C869–C877 (2018).
18. Hangarter, C. M. & Policastro, S. A. Electrochemical Characterization of Galvanic Couples Under Saline Droplets in a Simulated Atmospheric Environment. Corrosion 73, 268–280 (2016).
19. Chen, J., Dong, J., Wang, J., Han, E. & Ke, W. Effect of magnesium hydride on the corrosion behavior of an AZ91 magnesium alloy in sodium chloride solution. Corros. Sci. 50, 3610–3614 (2008).
20. Pourbaix, M. Atlas of electrochemical equilibria in aqueous solutions. Journal of Electroanalytical Chemistry and Interfacial Electrochemistry (National Association of Corrosion Engineers, 1967). doi:10.1016/0022-0728(67)80059-7
21. Schaller, R. Evaluating Stress Corrosion Cracking of Spent Nuclear Fuel Interim Storage Canisters. 1–71 (2019).
22. Chandran, R. R. & Chin, D. T. Reactor analysis of a chlor-alkali membrane cell. Electrochim. Acta (1986). doi:10.1016/0013-4686(86)80058-5

U.S. DEPARTMENT OF ENERGY
National Nuclear Security Administration
Sandia National Laboratories

Sandia National Laboratories is a multimission laboratory managed and operated by National Technology &Engineering Solutions of Sandia, LLC, a wholly owned subsidiary of Honeywell International Inc., for the U.S. Department of Energy's National Nuclear Security Administration under contract DE-NA0003525.
SAND No. _____